Prior activation state shapes the microglia response to antihuman TREM2 in a mouse model of Alzheimer's disease

Daniel C. Ellwanger[a,1], Shoutang Wang[b,1], Simone Brioschi[b], Zhifei Shao[c], Lydia Green[d], Ryan Case[e], Daniel Yoo[f], Dawn Weishuhn[d], Palaniswami Rathanaswami[d], Jodi Bradley[g], Sara Rao[c], Diana Cha[g], Peng Luan[h], Shilpa Sambashivan[a], Susan Gilfillan[b], Samuel A. Hasson[g], Ian N. Foltz[d], Menno van Lookeren Campagne[c,2], and Marco Colonna[b,2]

[a]Genome Analysis Unit, Amgen Research, Amgen Inc., South San Francisco, CA 94080; [b]Department of Pathology and Immunology, Washington University School of Medicine, St Louis, MO 63110; [c]Department of Inflammation and Oncology, Amgen Research, Amgen Inc., South San Francisco, CA 94080; [d]Department of Biologics Discovery, Amgen Research, Amgen Inc., Burnaby, BC, V5A1V7 Canada; [e]Discovery Attribute Sciences, Amgen Research, Amgen Inc., South San Francisco, CA 94080; [f]Department of Biologics Optimization, Amgen Research, Amgen Inc., Thousand Oaks, CA 91320; [g]Department of Neuroscience, Amgen Research, Amgen Inc., Cambridge, MA 02142; and [h]Department of Translational Safety and Bioanalytical Sciences, Amgen Research, Amgen Inc., Thousand Oaks, CA 91320.

Edited by Lawrence Steinman, Stanford University School of Medicine, Stanford, CA, and approved November 30, 2020 (received for review August 20, 2020)

Triggering receptor expressed on myeloid cells 2 (TREM2) sustains microglia response to brain injury stimuli including apoptotic cells, myelin damage, and amyloid β (Aβ). Alzheimer's disease (AD) risk is associated with the *TREM2*^{R47H} variant, which impairs ligand binding and consequently microglia responses to Aβ pathology. Here, we show that TREM2 engagement by the mAb hT2AB as surrogate ligand activates microglia in 5XFAD transgenic mice that accumulate Aβ and express either the common TREM2 variant (*TREM2*^{CV}) or *TREM2*^{R47H}. scRNA-seq of microglia from *TREM2*^{CV}-5XFAD mice treated once with control hIgG1 exposed four distinct trajectories of microglia activation leading to disease-associated (DAM), interferon-responsive (IFN-R), cycling (Cyc-M), and MHC-II expressing (MHC-II) microglia types. All of these were underrepresented in *TREM2*^{R47H}-5XFAD mice, suggesting that TREM2 ligand engagement is required for microglia activation trajectories. Moreover, Cyc-M and IFN-R microglia were more abundant in female than male *TREM2*^{CV}-5XFAD mice, likely due to greater Aβ load in female 5XFAD mice. A single systemic injection of hT2AB replenished Cyc-M, IFN-R, and MHC-II pools in *TREM2*^{R47H}-5XFAD mice. In *TREM2*^{CV}-5XFAD mice, however, hT2AB brought the representation of male Cyc-M and IFN-R microglia closer to that of females, in which these trajectories had already reached maximum capacity. Moreover, hT2AB induced shifts in gene expression patterns in all microglial pools without affecting representation. Repeated treatment with a murinized hT2AB version over 10 d increased chemokines brain content in *TREM2*^{R47H}-5XFAD mice, consistent with microglia expansion. Thus, the impact of hT2AB on microglia is shaped by the extent of TREM2 endogenous ligand engagement and basal microglia activation.

Alzheimer's disease | microglia | TREM2 | amyloid beta | monoclonal antibody

Alzheimer's disease (AD) is the most common cause of progressive dementia in older adults; it affects more than 5.5 million Americans, most 65 y of age or older, and represents the sixth leading cause of death in the United States (https://www.nia.nih.gov/health/alzheimers-disease-fact-sheet). The pathological features of AD include extracellular amyloid plaques composed of the amyloid β (Aβ) peptide, intraneuronal neurofibrillary tangles consisting of aggregated, hyperphosphorylated tau protein, neuroimmune activation, and reductions in synaptic density (1). Longitudinal natural history studies, such as the Alzheimer's Disease Neuroimaging Initiative, have demonstrated that deposition of Aβ in the central nervous system (CNS) occurs early in disease and is followed by tau pathology, consequently leading to neuronal cell death and cognitive impairment (2). Aβ accumulation also elicits a response by microglia, brain resident macrophages that support the development, function, and immune defense of the CNS (3).

While all dominant mutations causing familial early-onset AD occur either in the substrate (amyloid precursor protein, APP) or the proteases (presenilins) of the proteolytic pathway that generates Aβ (4), genome-wide association studies found many genetic polymorphisms linked with late-onset AD in genes expressed by microglia, such as triggering receptor expressed on myeloid cells 2 (TREM2), CD33, SPI1, SHIP1, and PLCγ2 (5, 6), providing strong evidence that microglia actively control the onset and/or progression of AD pathology (7). Microglia accumulate around Aβ plaques to contain and compact them, thereby

Significance

Alzheimer's disease (AD) is the most common dementia; no therapy halts its progression. AD pathology, including amyloid-β (Aβ) plaques, neurofibrillary tangles, and synapse loss, triggers microglial responses that modulate disease course. The TREM2 receptor promotes microglia responses to pathology and a variant, *TREM2*^{R47H}, impairs ligand binding and increases AD risk. Employing scRNA-seq, we asked: can an anti-TREM2 antibody, acting as a surrogate ligand, stimulate microglia in mice that accumulate Aβ and express either the common TREM2 variant (*TREM2*^{CV}) or *TREM2*^{R47H}? One systemic injection of anti-TREM2 restored microglia activation in *TREM2*^{R47H} mice but promoted limited activation in mice carrying *TREM2*^{CV}, which binds endogenous ligands. Thus, anti-TREM2 can strengthen microglial responses during AD, contingent on preexisting TREM2 engagement and basal activation.

Author contributions: S.W., I.N.F., M.v.L.C., and M.C. designed research; S.W., S.B., Z.S., L.G., R.C., D.Y., D.W., P.R., J.B., S.R., D.C., P.L., S.S., S.G., and S.A.H. performed research; D.C.E. and S.W. analyzed data; and D.C.E., S.W., M.v.L.C., and M.C. wrote the paper.

Competing interest statement: D.C.E., Z.S., L.G., R.C., D.Y., D.W., P.R., J.B., S.R., D.C., P.L., S.S., S.A.H., I.N.F., and M.v.L.C. are current employees or were past Amgen employees at the time when the experiments were performed. S.S. is Vice President of Nura Bio Inc. M.C. received research support from Amgen and serves on the Scientific Advisory Board of Vigil Neuroscience Inc.

This article is a PNAS Direct Submission.

[1]D.C.E. and S.W. contributed equally to this work.

[2]To whom correspondence may be addressed. Email: mvanlook@amgen.com or mcolonna@wustl.edu.

This article contains supporting information online at https://www.pnas.org/lookup/suppl/doi:10.1073/pnas.2017742118/-/DCSupplemental.

Published January 14, 2021.

reducing markers of axonal dystrophy in surrounding neurons (8). During this process, microglia modify their phenotypic and transcriptional properties, transitioning from a "homeostatic" to an activated profile often defined as disease-associated microglia (DAM) (6). This transition to the DAM phenotype is robustly activated in transgenic amyloid murine models of AD (9, 10) but is observed to a lesser extent in some human AD postmortem brains (11, 12), potentially reflecting insufficient microglial response to CNS damage in individuals who develop AD pathology.

Microglia transition to DAM has been shown to depend on TREM2, a macrophage cell surface receptor abundantly expressed in microglia (13). TREM2 is a member of the immunoglobulin superfamily that binds phospholipids, apoptotic cells, lipoproteins (such as high-density lipoprotein, low-density lipoprotein, and ApoE), and Aβ. TREM2 transmits intracellular signals through the associated adaptor DAP12, which recruits the protein tyrosine kinase Syk, leading to a cascade of protein tyrosine phosphorylation events that promote proliferation, survival, production of adenosine triphosphate, and protein biosynthesis. The ectodomain of TREM2 is cleaved from the cell surface by proteases, thereby limiting TREM2 signaling and releasing soluble TREM2 (sTREM2) (14, 15). Genetic variants in TREM2 are associated with multiple neurodegenerative diseases, including Nasu-Hakola disease, frontotemporal dementia, and AD. Because of its role in metabolic activation, TREM2 may function as a costimulatory molecule that sustains microglia activation during transition to DAM, which is initiated by various receptors engaged by CNS injury stimuli, such as Aβ, apoptotic cell debris, and myelin damage (13).

Several observations have suggested that activation of microglia through TREM2 may provide a promising therapeutic approach in AD. First, an arginine-to-histidine missense substitution at amino acid 47 (*TREM2*^{R47H}) that increases AD risk two to fivefold (16, 17), impairs ligand binding (18), and curtails microglia activation in humans (11) and mouse models of AD (8, 19). Second, complete deletion of *Trem2* in mice that accumulate Aβ plaques weakens microglial encapsulation of Aβ plaques, which enhances their neurotoxicity (20, 21), and blocks the conversion of microglia from homeostatic to DAM (9). Conversely, mice overexpressing TREM2 evince less Aβ-induced pathology (22). Finally, anti-TREM2 activating antibodies were recently shown to boost microglia responses to Aβ in vitro (23), moderate Aβ plaque load after short-term treatment (24), and promote microglia proliferation as well as attenuate the neurotoxic effects of Aβ plaques after long-term administration (25).

In this study, we characterized the biologic effects in the 5XFAD model of a new antihuman agonistic TREM2 mAb (hT2AB) and a murinized version of this agonist TREM2 mAb (mT2AB). This antibody binds the common TREM2 variant (*TREM2*^{CV}) and the AD-associated *TREM2*^{R47H} variant. hT2AB was tested in transgenic mice that express either *TREM2*^{CV} or human *TREM2*^{R47H} in place of endogenous *Trem2* (19). These mice were crossed with 5XFAD transgenic mice, which express human *APP* and *PSEN1* transgenes with a total of five AD-linked mutations that promote the accumulation of Aβ plaques (26). One feature of this model is a sex bias in amyloid pathology: female 5XFAD mice have more pronounced amyloid pathology than do males (27, 28).

We first showed that hT2AB is a TREM2 agonist which can cross the blood–brain barrier (BBB) after systemic administration. We next examined the effects of a single intraperitoneal injection of hT2AB or control hIgG1 on microglia by single-cell RNA seq (scRNA-seq). In control hIgG1-treated mice, microglia acquired a continuum of cell-state transitions from homeostatic toward four different types, including DAM, interferon-responsive (IFN-R) microglia, cycling microglia (Cyc-M), and MHC-II expressing (MHC-II) microglia, which likely reflected engagement of different signaling pathways. All trajectories required TREM2, as indicated by a significant enrichment of terminal microglial types in *TREM2*^{CV}-5XFAD mice compared to *TREM2*^{R47H}-5XFAD and *Trem2*$^{-/-}$-5XFAD mice. Further, Cyc-M and IFN-R microglia were more abundant in females than males, which correlated with a higher degree of Aβ accumulation in females. hT2AB promoted cell cycle re-entry in *TREM2*^{R47H}-5XFAD mice and promoted Cyc-M expansion more effectively in males than in females within the *TREM2*^{CV}-5XFAD cohort. Likewise, hT2AB induced the terminal IFN-R population in *TREM2*^{R47H}-5XFAD of both sexes, as well as *TREM2*^{CV}-5XFAD males, but did not promote this cell fate in *TREM2*^{CV}-5XFAD females, in which this population was already robustly induced. Thus, mAb-mediated engagement of TREM2 mainly increased Cyc-M and IFN-R fates in microglia where TREM2 engagement is deficient or suboptimal. Analysis of expression dynamics of individual genes showed that hT2AB costimulated expression changes as soon as cell fates were determined but did not alter the transcriptional identity of the terminal cell types.

We finally tested the effect of mT2AB on brain biochemical analytes and histological images in the 5XFAD mice after repeated injections every 3 d for a short period of time. mT2AB treatment resulted in the greatest increases in CCL4, CXCL10, and IL-1β, which are produced by microglia, in *TREM2*^{R47H}-5XFAD mice. This is consistent with the scRNA-seq data suggesting that mT2AB induces greater activation of microglia in *TREM2*^{R47H}-5XFAD than in *TREM2*^{CV}-5XFAD mice. Female 5XFAD mice carrying *TREM2*^{R47H} and *TREM2*^{CV} showed greater levels of amyloid deposition relative to their male counterparts, which is consistent with the observations of greater hT2AB-induced shifts in males versus females. We conclude that the amplitude of hT2AB-mediated effects on microglia is shaped by their basal cycling and differentiation status, preexisting TREM2 engagement and basal microglia activation prior to mAb-mediated stimulation.

Results

hT2AB Is an Agonistic mAb Specific for Human TREM2. hT2AB was generated by gene gun-mediated immunization of XenoMouse animals (29) with complementary DNA (cDNA) encoding human *TREM2* and *DAP12*. Monoclonal antibody hT2AB was selected from a panel of agonistic anti-TREM2 antibodies. hT2AB selectively bound purified human TREM2 (affinity (K_D) = 50 nM) (Fig. 1*A*). Functional potency was determined by pSyk induction in HEK293 cells expressing human TREM2 and DAP12 (clone G13) and in human monocyte–derived macrophages (hMacs), revealing an EC_{50} of 222 pM and 166 pM, respectively (Fig. 1 *B* and *C*). hT2AB induction of intracellular signaling depended on bivalent binding and cross-linking of TREM2, as demonstrated by the lack of activity of its monomeric antigen-binding fragment (Fab) (Fig. 1*D*). Furthermore, release of sTREM2 following stimulation of hMacs was reduced by hT2AB (Fig. 1*E*).

To examine the effect of hT2AB-mediated activation of TREM2 on primary macrophages, hMacs were stimulated with hT2AB, isotype control, or acetylated LDL as a positive control, followed by assessment of chemokines released in culture supernatants at various timepoints after stimulation. hT2AB induced a time-dependent increase in the amount of CCL4 released by human macrophages (Fig. 1*F*), demonstrating that hT2AB activates primary macrophages. We previously showed that TREM2 enables macrophage survival in cultures with limiting concentrations of CSF1 (30), and tool mouse TREM2 antibodies that induce pSyk also boost in vitro survival of macrophages under the same challenge conditions (23). Thus, we also tested whether hT2AB impacts in vitro survival of macrophages after CSF1 withdrawal. We prepared bone marrow macrophages (BMMs) from *TREM2*^{CV} mice by culture with CSF1 and then tested their survival in the presence or absence of hT2AB 48 h after removal of CSF1 from the medium (Fig. 1*G*). Indeed, hT2AB sustained survival of BMM in a dose-dependent manner.

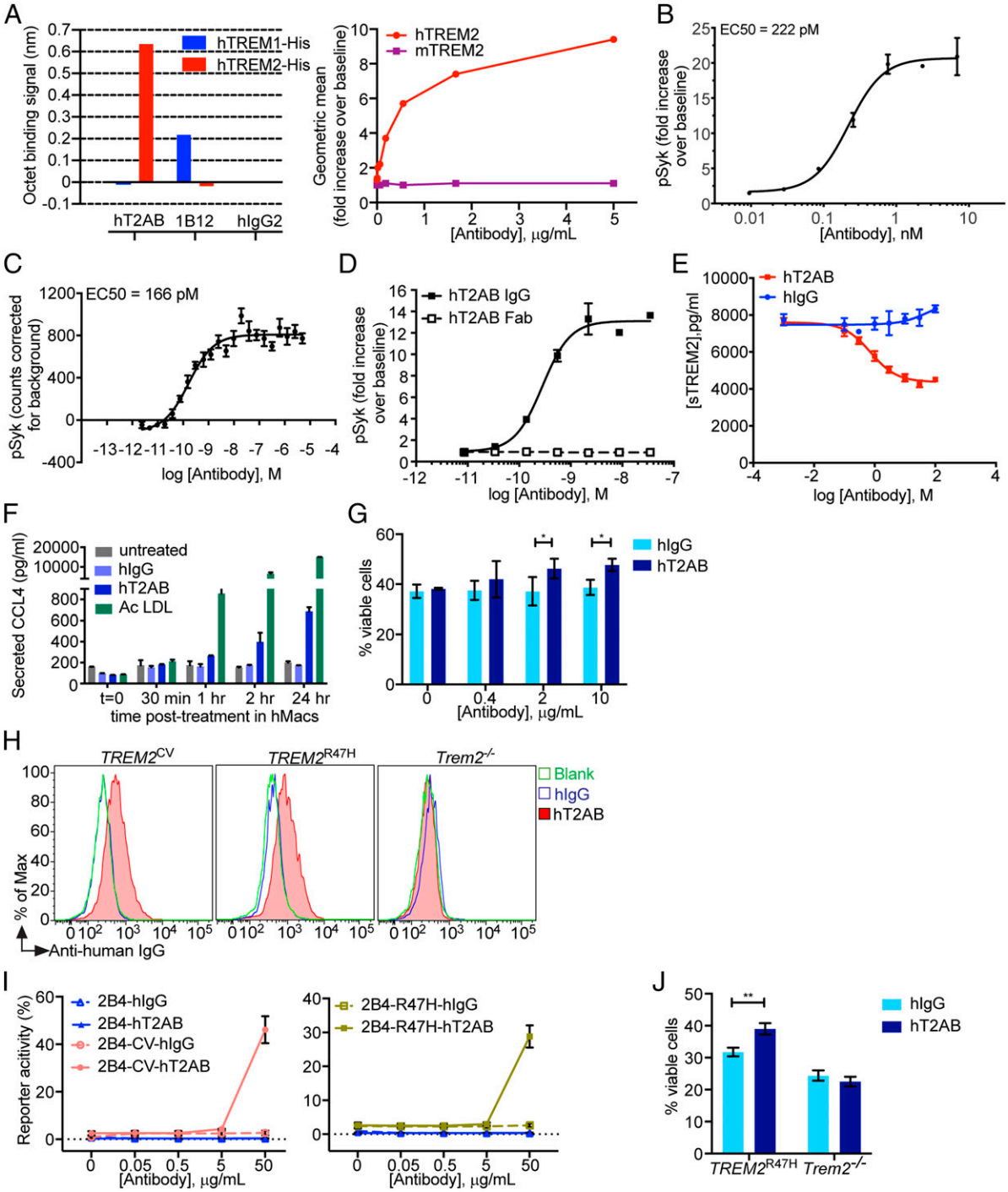

Fig. 1. hT2AB is a hTREM2 agonistic antibody. (*A*) hT2AB specifically binds to hTREM2 but does not bind to hTREM1 or mTREM2. The data show the binding signals of hTREM2-His to hT2AB measured by Octet. 1B12 is an anti-hTREM1 antibody that binds exclusively to hTREM1-His. There is no binding to either hTREM1-His or hTREM2-His to irrelevant hIgG2 (*Left*). hT2AB binds to hTREM2 transiently coexpressed with hDAP12 in HEK293 cells but does not bind to HEK293 cells that express mTREM2 and mDAP12 as measured by flow cytometry (*Right*). (*B*, *C*) Functional EC50 of hT2AB in HEK293 cells stably expressing hTREM2 and hDAP12 (clone G13) (*B*) and hMacs (*C*). Activation of hTREM2 was determined by measuring the induction of Syk phosphorylation (pSyk) after exposure of cells to different concentrations of hT2AB ($n = 8$). (*D*) Activation of hTREM2 by hT2AB IgG1 and hT2AB Fab was determined by measuring Syk phosphorylation in clone G13 exposed to different concentrations of antibodies ($n = 3$). (*E*) Quantification of sTREM2 in conditioned media from hMacs treated with different concentrations of hT2AB or control hIgG1 antibody for 24 h without any immune challenge ($n = 4$ for each group). (*F*) Quantification of CCL4 in conditioned media from hMacs treated with hT2AB or control hIgG1 antibody at 200 nM at different time points. Acetylated LDL was used as a positive control ($n = 2$ for each group). (*G*) Cell viability assay of BMMs from *TREM2*^{CV} mice after CSF1 withdrawal were treated with different concentrations of plate bound hT2AB or control hIgG1 for 48 h ($n = 3$ for each group). (*H*) Binding assay of hT2AB for BMMs from *TREM2*^{CV} and *TREM2*^{R47H}. BMMs from *Trem2*$^{-/-}$ were used as a negative control. (*I*) 2B4 reporter cell lines expressing hTREM2 (CV or R47H) were stimulated with different amounts of plate bound hT2AB or control hIgG1. GFP expression was measured by flow cytometry ($n = 2$ for each group). (*J*) Cell viability of BMMs from *TREM2*^{R47H} mice after CSF1 withdrawal treated with plate bound hT2AB or control hIgG1 at 10 μg/mL for 48 h. $^{*}P < 0.05$; $^{**}P < 0.01$ by two-way ANOVA with Sidak's multiple comparisons test. All data in Fig. 1 are shown as mean ± SD except for *B* and *C*, which depict mean ± SEM.

https://doi.org/10.1073/pnas.2017742118

Finally, we sought to determine whether the AD-associated R47H mutation affects hT2AB binding and/or signaling. First, we demonstrated that hT2AB stained BMM prepared from both *TREM2*^{CV} and *TREM2*^{R47H} mice (Fig. 1*H*). Then, we tested whether hT2AB can induce the expression of GFP in the Ca^{2+}-NFAT–driven reporter cell line 2B4 stably transfected with either *TREM2*^{CV} or *TREM2*^{R47H} together with DAP12 (Fig. 1*I*) (18). hT2AB induced GFP in both *TREM2*^{CV} and *TREM2*^{R47H} transfected reporter cells. Moreover, hT2AB sustained survival of BMM derived from *TREM2*^{R47H} mice cultured without CSF1 (Fig. 1*J*), conclusively demonstrating that hT2AB activates both TREM2^{CV} and TREM2^{R47H}.

hT2AB Can Cross the BBB and Attain Effective Brain Concentrations. Since peripherally administered mAbs cross the BBB poorly, we performed pharmacokinetic/pharmacodynamic studies to define a dosing scheme that ensures effective concentrations of hT2AB in the brain. Groups of *TREM2*^{CV}, *TREM2*^{R47H}, and *Trem2*$^{-/-}$ mice were injected intravenously (i.v.) with different doses of hT2AB. After 24 h, we measured the concentrations of CXCL10, CCL4, CCL2, CXCL2, and CST7 by Meso Scale Discovery (MSD) in brain lysates as proxies of microglia activation. hT2AB amplified all parameters at a dose between 30 to 100 mg/kg (Fig. 2 *A*–*E*). *TREM2*^{R47H} mice were slightly more responsive than *TREM2*^{CV} mice. No response above baseline was noted in *Trem2*$^{-/-}$ mice. A time course of hT2AB concentration in the brain lysates after single i.v. injection of 30 mg/kg in *TREM2*^{R47H} and *Trem2*$^{-/-}$ mice revealed that the hT2AB brain concentration was 25-fold higher than its EC_{50} in clone G13 at all time points (4, 8, and 24 h) (Fig. 2*F*). Accordingly, an increase of *Cxcl10*, *Ccl2*, *Ccl4*, *Cst7*, and *Tmem119* messenger RNAs was detectable in lysates of *TREM2*^{R47H} but not *Trem2*$^{-/-}$ brains 8 h after injection and further increased after 24 h (Fig. 2 *G*–*K*). We conclude that a single injection of 30 mg/kg of hT2AB is sufficient to activate microglia in vivo for at least 24 h.

scRNA-Seq Reveals Four Microglia Trajectories in Control hIgG1-Treated *TREM2*^{CV}-5XFAD Mice. To examine the impact of hT2AB on microglia in vivo, we resorted to scRNA-seq. We injected a single dose of hT2AB or control hIgG1 into the peritoneal cavity of 8mo-old 5XFAD mice crossed to either *TREM2*^{CV} (*TREM2*^{CV}-5XFAD) or *TREM2*^{R47H} (*TREM2*^{R47H}-5XFAD) mice. Both females and males were included, and we also injected female *Trem2*$^{-/-}$ mice to control for off target effects of hT2AB (Fig. 3*A*). Mice were killed 48 h after injection. Assessment of antibody levels in the cerebellum confirmed that hT2AB crossed the BBB and reached the brain parenchyma (*SI Appendix*, Table S1). CD45^{+} cells were isolated from brain cortices and submitted for scRNA-seq using the 10× Genomics Chromium platform (Fig. 3*A*). A total of 71,303 cells passed a rigorous multistep quality control process (*SI Appendix*, Fig. S1). We applied a supervised approach to initially classify cells into major immune cell subtypes by matching single-cell expression profiles to ImmGen gene signatures (31) (Fig. 3*B*). A lower-dimensional latent space correcting for treatment, sex, and genotype covariates, as well as blocking technical confounders, was derived from the cellular expression profiles. A graph encoding cellular relationships was generated using the Jaccard similarity coefficient on each cell's nearest neighborhood and unbiasedly segmented using Louvain's community detection method. Each cell was assigned to the most enriched cell type in its segment resulting in a total classification of 10 major immune cell populations (Fig. 3 *C*–*E*). Microglia accounted for more than 90% of total cells. The remaining cells were composed of T cells, macrophages, dendritic cells, monocytes, B cells, neutrophils, cycling cells, and fibroblasts, as well as a population of cells that had a mixed expression profile of macrophages and T cells, perhaps capturing the interaction of T cells infiltrating the brain of mice accumulating Aβ (Dataset S1) (32). Microglia differentially expressed common marker genes, including *P2ry12*, *Hexb*, *Tmem119*, and *C1q* family genes, among others, that were absent in other cell populations (Fig. 3 *F* and *G*). These genes were also preferentially expressed in a small cluster identified as perivascular macrophages that had increased *Mrc1* and *Pf4* expression. Notably, monocytes and perivascular macrophages were not found to be significantly impacted due to hT2AB treatment. The relative fraction of sampled monocytes or perivascular macrophages from mice treated with either control hIgG1 or hT2AB remained unchanged (hIgG1/hT2AB ratio for monocytes: *TREM2*^{CV}-5XFAD = 1.3%/0.9%, *TREM2*^{R47H}-5XFAD = 1.0%/0.9%, *Trem2*$^{-/-}$-5XFAD = 0.7%/0.4%; macrophages: *TREM2*^{CV}-5XFAD = 3.0%/3.0%, *TREM2*^{R47H}-5XFAD = 2.4%/2.4%, *Trem2*$^{-/-}$-5XFAD = 2.3%/1.8%), and no genes were found differentially expressed between treatment cohorts (absolute effect size threshold >1.5).

We next defined the baseline heterogeneity for 5,694 microglia cells from control hIgG1–injected *TREM2*^{CV}-5XFAD mice. We used diffusion maps to learn a lower-dimensional manifold best representing the latent temporal axis in the data. Clustering using Louvain's community detection method revealed 11 cell states, which were subsequently unbiasedly placed along a maximum parsimony tree resembling branching cell activation continua. The resulting trajectory originated from homeostatic microglia (highly expressing *Tmem119*, *P2ry12*, and *Cx3cr1*), progressed through five intermediate stages of differentiation (t1 through t5) and then branched into four distinct terminal types: IFN-R, MHC-II, Cyc-M, and a t6 stage that further differentiated into a DAM cluster (Fig. 4*A* and Dataset S1). By scoring transcriptome similarities and inequalities with the DAM reported by Keren-Shaul et al. (9), we found an increasing expression resemblance along the trajectory from t1 to t6 and DAM clusters reported here, culminating in a significant similarity between terminal DAMs from both studies (P value = 1.4×10^{-19}; Fig. 4*B*). We predicted the cell cycle state of each cell using a machine-learning method that was trained on pairs of cell cycle state marker expression (33). Cyc-M evinced a significant enrichment of cells (63.0%) in growth (G)2/mitotic (M) phase across all clusters (average percentage in remaining clusters = 1.1%; Fig. 4*C*). IFN-R microglia most abundantly expressed interferon-stimulated genes (ISG), such as *Bst2*, *Ifit3*, *Ifitm3*, and *Isg15* (Fig. 4*D*). Gene Ontology terms enrichment analysis corroborated the expression of a gene program induced by IFNs, particularly type I IFNs (i.e., IFNα and IFNβ) (*SI Appendix*, Fig. S2). Among all clusters, MHC-II microglia expressed the highest levels of MHC class II pathway genes, together with classical and nonclassical MHC class I genes (Fig. 4*E*). Interestingly, this subset also expressed high levels of GPI-linked *Cd52* and *Ly6e*, both of which have been associated with immunoregulation (34). Notably, IFN-imprinted and MHC-II–presenting clusters were previously reported in another mouse AD model (35). Overall, our unbiased baseline scRNA-seq analysis of microglia in control hIgG1-treated *TREM2*^{CV}-5XFAD mice revealed four distinct fates in the microglial response to Aβ plaques, which may reflect the engagement of different signaling pathways.

TREM2 Variants Profoundly Impact Microglia Trajectories. We intended to perform an integrative analysis on the impact of sex, genotype, and treatment on the differentiation of DAM, Cyc-M, IFN-R, and MHC-II microglia. For this purpose, we employed a machine learning–based approach to harmonize samples (*SI Appendix*, Fig. S3), and we inferred trajectories from the branching cluster, t5, to each terminal end by fitting principal curves on the learned nonlinear manifolds of all cells from all conditions (Fig. 5*A*). Using this method, we first assessed the baseline impact of *TREM2*^{CV}-5XFAD and *TREM2*^{R47H}-5XFAD genotypes on microglial trajectories. We particularly focused on

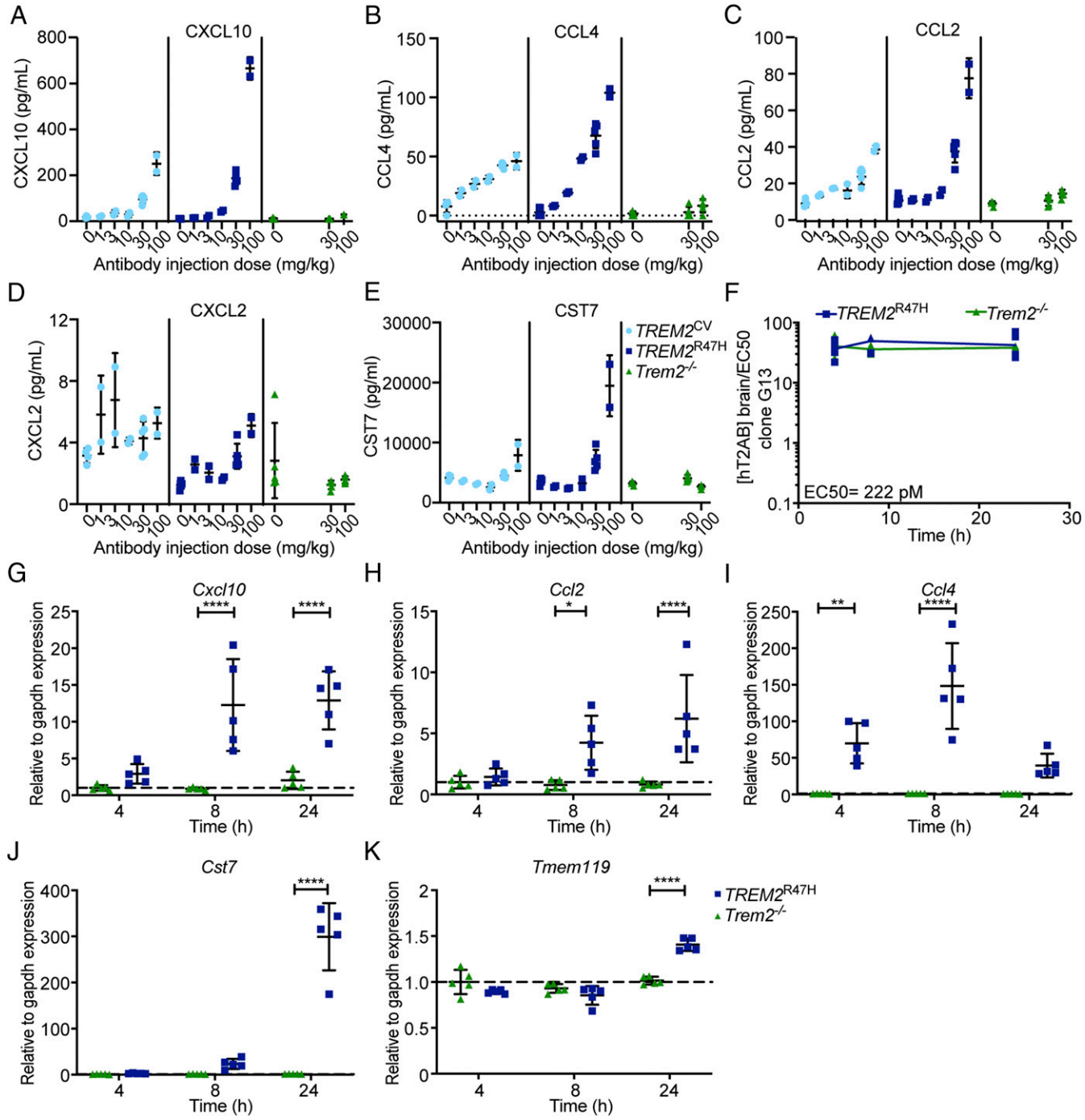

Fig. 2. Pharmacokinetics and pharmacodynamics of hT2AB. (*A–E*) Pharmacodynamic study of hT2AB in *TREM2*^{CV}, *TREM2*^{R47H}, or *Trem2*$^{-/-}$ male mice. Different mouse cohorts received a single dose of hT2AB i.v. in the range of 0 (vehicle) to 100 mg/kg for 24 h. Concentrations of chemokines, including CXCL10 (*A*), CCL4 (*B*), CCL2 (*C*), and CXCL2 (*D*), as well as a microglia activation biomarker CST7 (*E*), were measured by MSD technology in brain lysates (vehicle, $n = 4$ for *TREM2*^{CV}, $n = 5$ for *TREM2*^{R47H} or *Trem2*$^{-/-}$; 1, 3, and 10 mg/kg, $n = 2$ for *TREM2*^{CV} or *TREM2*^{R47H}; 30 mg/kg, $n = 5$ for all three genotypes; 100 mg/kg, $n = 2$ for *TREM2*^{CV} or *TREM2*^{R47H}, $n = 5$ for *Trem2*$^{-/-}$). (*F–K*) A single dose of hT2AB was administered i.v. in *TREM2*^{R47H} or *Trem2*$^{-/-}$ male mice at 30 mg/kg. Different mouse cohorts were killed 4, 8, and 24 h after antibody treatment, and brain tissues were collected and lysed for measurement of hT2AB antibody levels and expression of microglial activation biomarkers ($n = 5$ for each group). (*F*) hT2AB brain concentration (nanomolar) is ~25-fold higher than the EC_{50} values for Syk phosphorylation (222 pM) in clone G13 up to 24 h after i.v. administration of 30 mg/kg hT2AB. qRT-PCR analysis showed increased expression of *Cxcl10* (*G*), *Ccl2* (*H*), *Ccl4* (*I*), and *Cst7* (*J*), as well as the homeostatic microglia marker *Tmem119* (*K*), upon hT2AB treatment. *$P < 0.05$; **$P < 0.01$; ****$P < 0.0001$ by two-way ANOVA with Sidak's multiple comparisons test; all data are shown as mean ± SD.

females because they have more pronounced Aβ deposition than males (27, 28). Further, we included *Trem2*$^{-/-}$-5XFAD mice for further comparison. We split each cell type trajectory into 10 equally sized pseudotime intervals and quantified the number of cells from control hIgG1-treated female mice per interval. Proportions of cell populations were estimated using a Bootstrapping method to account for technical variance between replicates (Fig. 5 *B–E*). We found that for all four terminal time

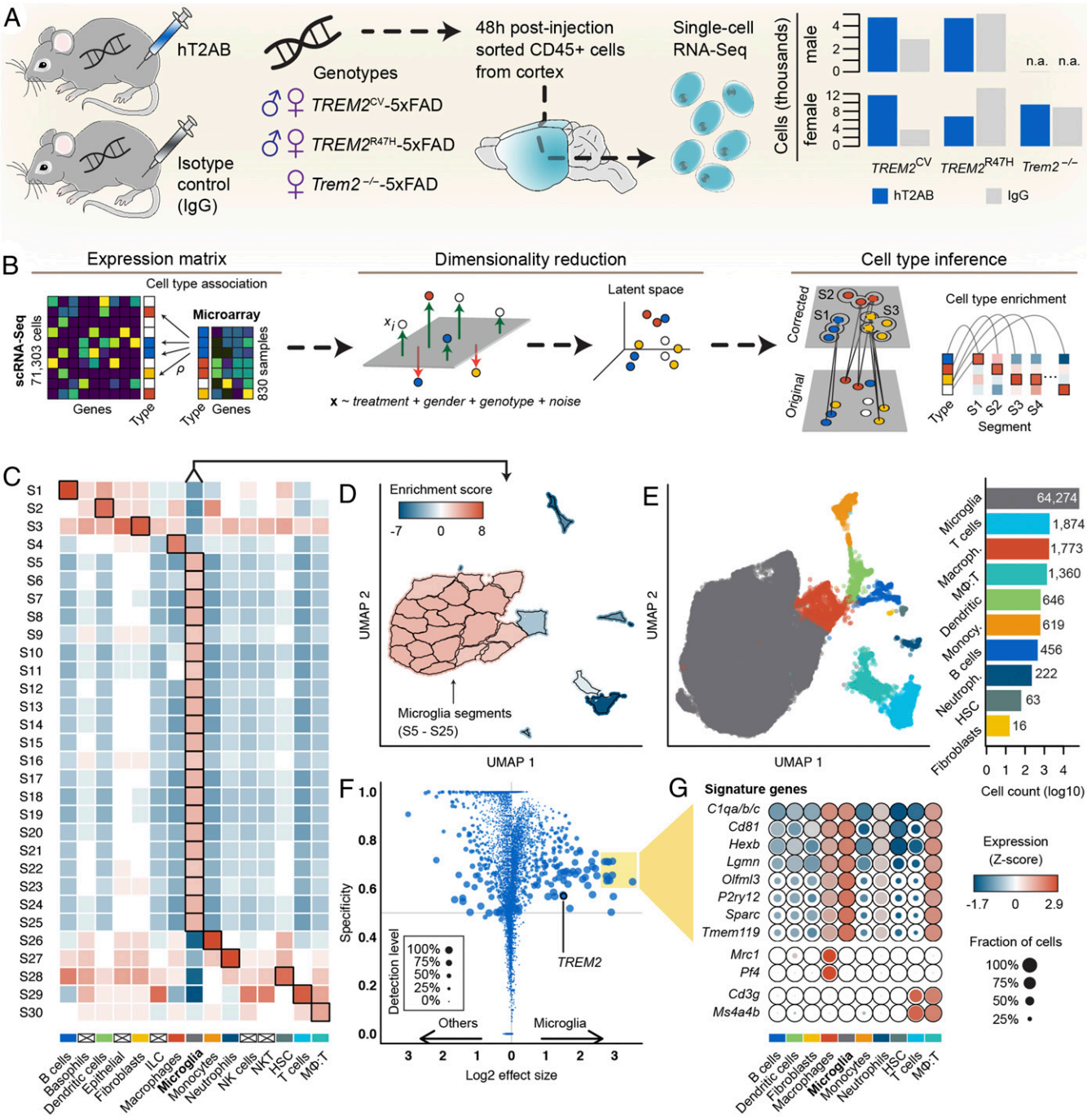

Fig. 3. Sampling microglia from the human TREM2-5XFAD mouse models. (*A*) Two days after antibody injection, CD45+ cells were collected from cortex of male and female 5XFAD mice with endogenous Trem2 knockout (*Trem2*$^{-/-}$) with or without one of two variants of a human TREM2: CV and R47H. A total of 71,303 cells passed scRNA-seq quality control. (*B–D*) Supervised immune cell type classification. Individual cells were assigned a similarity score to 830 microarray samples of sorted mouse immune cells generated by the Immunologic Genome (ImmGen) Project. Cells were embedded in a lower-dimensional latent space while blocking observed covariates. Cell type labels were corrected by the enriched cell type of each segment of the latent space. (*E*) Uniform manifold approximation and projection of all cells representing the global data structure; cells are colored by the 10 identified immune cell types. (*F*) Differential gene expression of microglia. Absolute differences in expression levels to other CD45+ cells are quantified by effect size; gene expression specificity and gene detection rate were determined using conditional probabilities with uniform priors for cell types to avoid sample size bias. Specificity is defined by the posterior probability that a cell is of a certain cell type given it is expressing a particular gene; the detection level is defined by the relative fraction of cells expressing a particular gene. (*G*) Expression profiles of 13 microglia signature genes meeting the specificity threshold of 0.6 and an effect size threshold of 2.5, and perivascular gene markers *Mrc1* and *Pf4*, as well as T cell markers *Cd3g* and *Ms4a4*; the mean expression of the Complement C1q subcomponents a, b, and c is shown.

intervals, *TREM2*^{CV}-5XFAD mice had the highest fraction of cells (estimated mean ± SE of 95% CI, DAM: 15.5 ± 0.1%, Cyc-M: 13.9 ± 0.1%, IFN-R: 22.3 ± 0.2%, and MHC-II: 5.6 ± 0.1%). This corroborated that TREM2 is required for full differentiation of DAM, consistent with previous studies (9), and extended this concept to the Cyc-M, IFN-R, and MHC-II fates induced by Aβ

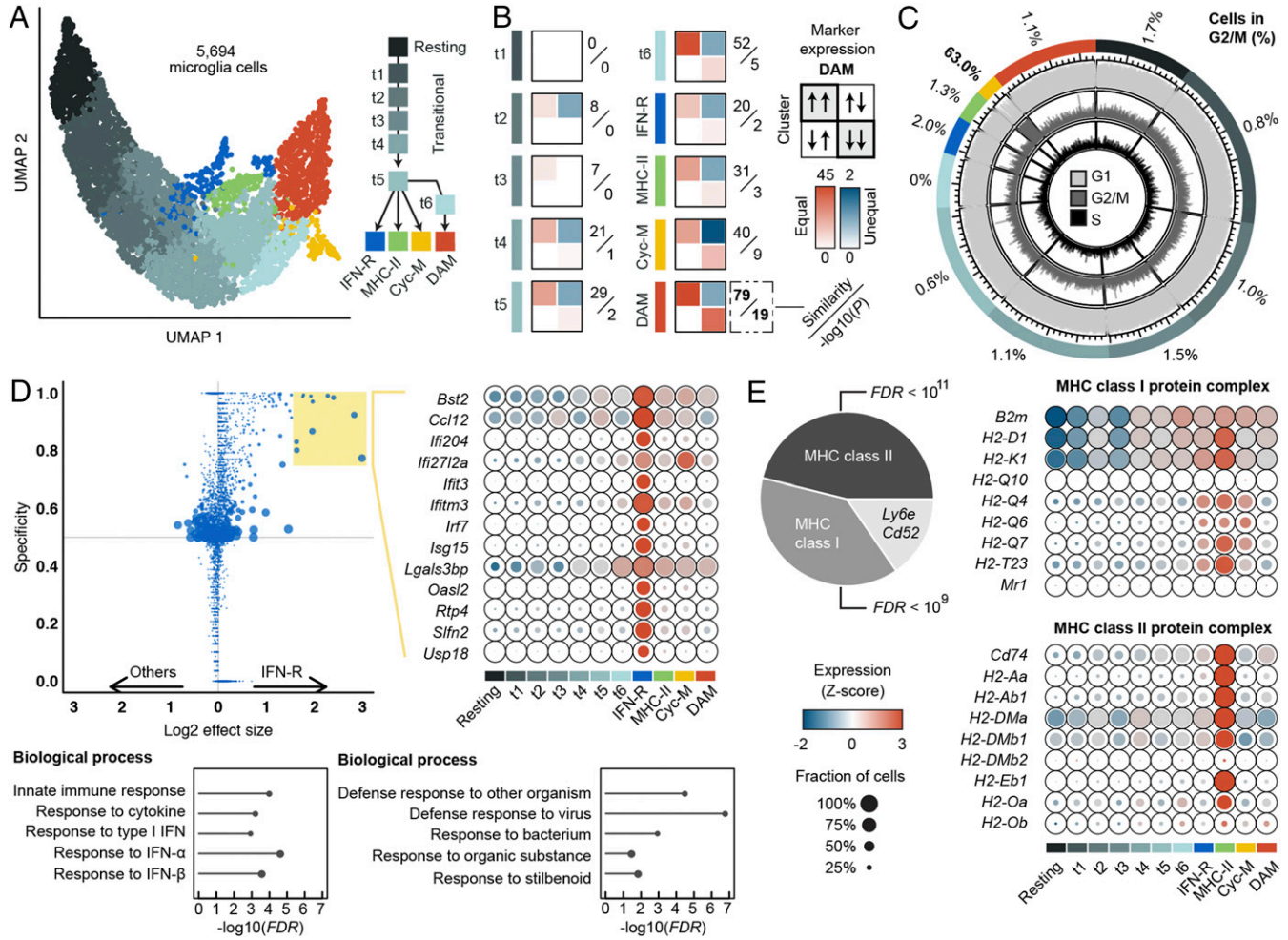

Fig. 4. Characterization of activated microglia populations. (*A*) Unsupervised clustering identified 10 distinct subpopulations spanning a trajectory from homeostatic microglia toward four terminal phenotypes. (*B*) Contingency tables counting agreements (diagonal) and disagreements (off-diagonal) between the expression profile of the DAM population described by Keren-Shaul et al. (9) and each cluster in this study; quantifications are based on (log2) 0.5-fold up- and down-regulated genes relative to the homeostatic population. A similarity score is calculated by subtracting the off-diagonal values from the sum of the diagonal values; *P* values are calculated testing the overall agreement between both studies. Increasing gene expression similarities along the trajectory from t1 via t6 to the DAM cluster, highlighted in red, can be observed. (*C*) Scoring of cell cycle states. Each cell was predicted to be either in G1, G2/M, or S phase using machine learning. One cluster highlighted in yellow, Cyc-M, shows strong enrichment of cycling cells. (*D*) Differential expression analysis reveals one cluster, IFN-R, that shows enrichment of genes related to the interferon pathway (*D*), and one cluster, MHC-II, enriched in genes encoding members of the MHC class II protein complex (*E*). The expression of selected marker genes is shown in *D*, and all MHC class I/II genes as annotated in the GO are shown in *E*. Fisher's exact test with false discovery rate (FDR) correction was used for GO term enrichment analysis.

accumulation. *TREM2*^{R47H}-5XFAD mice harbored more late-stage DAMs and MHC-II cells (DAM: 7.3 ± 0.1%, Cyc-M: 4.1 ± 0.1%, IFN-R: 10.3 ± 0.1%, and MHC-II: 1.7 ± 0.1%) than did *Trem2*$^{-/-}$-5XFAD mice (DAM: 5.0 ± 0.0%, Cycling: 4.8 ± 0.1%, IFN-R: 12.7 ± 0.1%, and MHC-II: 0.0 ± 0.0%). This is in agreement with previous findings reporting that the *TREM2*^{R47H} mutant, although hypomorphic, is a partial loss-of-function with limited capacity to induce DAM maturation (19). Since *TREM2*^{R47H} poorly binds lipid ligands, constant TREM2 interaction with endogenous ligands is required to sustain the differentiation of DAM and to a minor extent MHC-II microglia.

Female Microglia Are Prone to Cyc-M and IFN-R Fates in Control hIgG1-Treated *TREM2*^{CV}-5XFAD Mice. We compared the impact of sex on microglial trajectories in *TREM2*^{CV}-5XFAD mice. We did not observe a difference in proportions of late-stage DAMs (estimated mean± SE of 95% CI, females: 15.5 ± 0.1%, males: 14.5 ± 0.1%; *SI Appendix*, Fig. S4*A*). However, the representation of Cyc-M, IFN-R, and (to a minor extent) MHC-II cell types was biased. The relative fraction of cells in the terminal Cyc-M (*SI Appendix*, Fig. S4*B*) and IFN-R (*SI Appendix*, Fig. S4*C*) interval was considerably higher in females than in males (Cyc-M female: 13.9 ± 0.1%, male: 8.1 ± 0.1%; IFN-R female: 22.3 ± 0.2%, male: 17.0 ± 0.2%). Estimated terminal MHC-II cell fractions indicated a moderate tendency of this cell type to be more abundant in males than in females (female: 5.6 ± 0.1%, male: 8.0 ± 0.2%; *SI Appendix*, Fig. S4*D*).

We also assessed the gene expression dynamics of the top 10 signature genes for each terminal type before and after the branching cluster t5 (*SI Appendix*, Fig. S4 *A–D*). Gene expression was modeled as a function of pseudotime using negative binomial generalized additive models (36). This allows evaluation of gene expression patterns along the differentiation trajectory on a single-cell level and, therefore, independent of cell sampling densities. For each microglia type, signature genes showed a similar consecutive up-regulation pattern toward the terminal end of each trajectory in both sexes. This implies that microglia types exhibit similar transcriptome compositions and, thus,

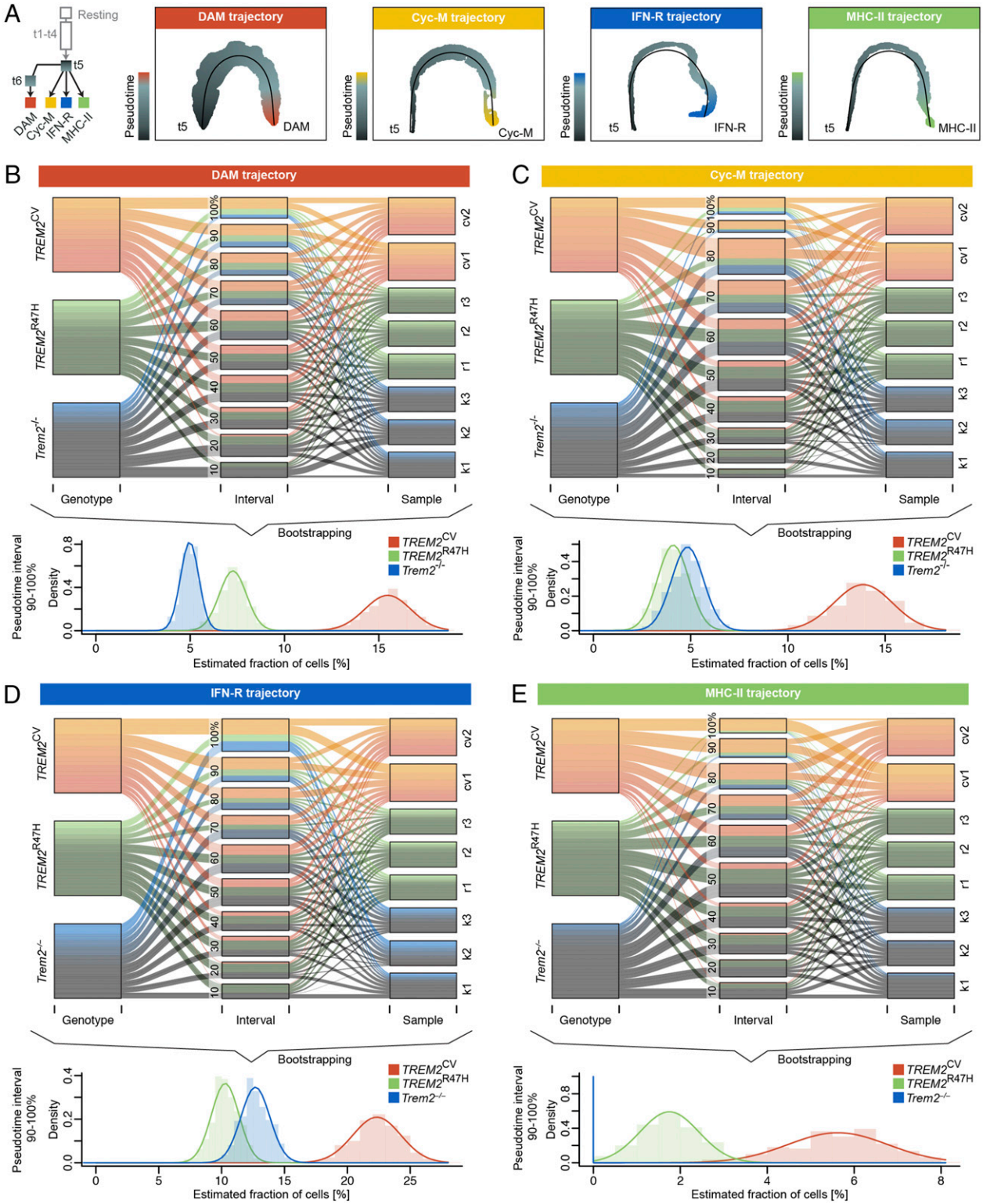

Fig. 5. Genotype-driven effects on microglia fates. (*A*) Trajectory tree and visualization of computed linear trajectories from t5 toward each terminal microglia type. Pseudotime was inferred by fitting principal curves (black lines) in the lower dimensional manifold. Each datapoint represents a cell colorized by its pseudotemporal location along the trajectory. (*B–E*) Alluvial plots showing the relative fraction of each genotype and its replicates over all pseudotime intervals (*Upper*); representation was corrected for different samples sizes. The lower image shows the distributions of estimated fractions of cells in the 90 to 100% pseudotime interval using Bootstrapping (*Lower*).

potentially perform qualitatively identical functions in males and females. However, microglia may be primed differently, prompting a more dynamic microglial response, which ultimately results in a quantitative shift in the microglia population landscape between sexes. For example, the basal expression level of the interferon-stimulated gene *Ifi27l2a* was elevated in female

mice along the Cyc-M and the IFN-R trajectory (Wald test on early and late terminal differences: Cyc-M P value early = 9.9×10^{-9}, late = 3.8×10^{-1}; IFN-R P value early = 1.0×10^{-4}, late = 1.8×10^{-2}; *SI Appendix*, Fig. S4*B*). *Ifi27l2a* is a regulator of the transcriptional activity of NR4A nuclear receptors, which coordinate cellular and systemic metabolic processes (37), as well as myeloid cell differentiation and their response to inflammatory stimuli (38–40). An induced basal expression level of *Ifi27l2a* may indicate increased cellular exposure to pathophysiological environmental cues. In fact, previous studies have shown that female 5XFAD mice accumulate more Aβ than male 5XFAD mice (27, 28). Accordingly, we also detected more insoluble Aβ in the brain of female than male *TREM2*^{CV}-5XFAD mice (*SI Appendix*, Fig. S4*E*). Thus, altogether, these data suggest that the enrichment of IFN-R and Cyc-M types in female *TREM2*^{CV}-5XFAD mice reflects a microglial response to more copious Aβ aggregates.

hT2AB Effects on Cyc-M, IFN-R and MHC-II Fates Depend on Preexistent Microglia State. We next examined how hT2AB impacts microglial fates compared to control hIgG1 in *TREM2*^{CV}-5XFAD and *TREM2*^{R47H}-5XFAD mice of both sexes. To account for off-target treatment effects, we included data from treatment-matched *Trem2*$^{-/-}$-5XFAD mice. hT2AB did not induce expansion of DAM (estimated ratio of control hIgG1 to hT2AB cell fractions in the 90 to 100% pseudotime interval, R, of *TREM2*^{CV}/*TREM2*^{R47H}/*Trem2*$^{-/-}$-5XFAD females: R = 0.6/1.0/0.9, males: R = 1.0/1.0/not applicable). Interestingly, hT2AB treatment of *TREM2*^{CV}-5XFAD mice activated cell cycle reentry of microglia in males (R = 4.2), but microglia did not undergo additional cell cycle induction in females (R = 0.5; Fig. 6*A*). An increased magnitude of proliferative response to hT2AB was evident in microglia from *TREM2*^{R47H}-5XFAD, as this population expanded in both female and male mice (female: R = 4.9, male: R = 7.9). Likewise, hT2AB induced the terminal IFN-R population in *TREM2*^{CV}-5XFAD males (R = 1.3), *TREM2*^{R47H}-5XFAD males (R = 2.1), and *TREM2*^{R47H}-5XFAD females (R = 3.2) but did not promote this cell fate in *TREM2*^{CV}-5XFAD females (R = 0.9). Given that control hIgG1–treated *TREM2*^{R47H}-5XFAD mice have fewer Cyc-M and IFN-R microglia than *TREM2*^{CV}-5XFAD mice and a similar disproportion is evident between *TREM2*^{CV}-5XFAD males and females, our result suggests that hT2AB activates both microglial proliferation and IFN-R differentiation either when acting as a surrogate ligand for *TREM2*^{R47H} or when Aβ accumulation is still limited. hT2AB does not appear to further increase the percentage of activated microglia beyond the robust induction of these activation states in female 5XFAD mice carrying *TREM2*^{CV}. MHC-II microglia, which were relatively scarce in *TREM2*^{CV}-5XFAD mice of both sexes (though more were found in males than in females) underwent hT2AB-induced expansion in both sexes, but the response was more pronounced in females (female: R = 4.9, male: R = 1.9). Similarly, hT2AB enlarged the late-stage MHC-II populations in *TREM2*^{R47H}-5XFAD mice of both sexes (estimated ratio of control hIgG1 to hT2AB cell fractions in the 80 to 100% pseudotime interval of females: 4.1, males: 2.1). Overall, hT2AB triggered microglial cell cycle reentry and replenished the IFN-R and MHC-II cell pools in *TREM2*^{R47H}-5XFAD mice. In *TREM2*^{CV}-5XFAD mice, hT2AB-induced effects were driven by preexisting cell type compositions toward restoration of less abundant populations.

Anti-TREM2 Costimulates the Expression of Single Genes within Terminal Microglia Types. Since our data described a developmental continuum, microglia clusters represented a mixture of cells, each encompassing a discrete quantity captured at different developmental stages. Thus, by comparing the cell clusters, gene expression differences would be obscured. To avoid this problem, we fitted the gene expression dynamics of each cell as it differentiates from the branching point toward a terminal phenotype. The resulting expression model was independent of sampled cell fractions along the trajectory, allowing us to pinpoint underlying differential gene expression. Robustly detected genes were filtered per trajectory. We statistically compared the early start and the late end of each lineage between hT2AB- and control hIgG1–treated mice (Fig. 6*B* and Dataset S2). Most hT2AB-induced gene expression changes occurred early in the pseudotime trajectory (mean = 76.8%), while only a minority of these changes was manifest in the terminal cell type (mean = 19.1%). This indicated that transcriptional shifts are mainly transient and that hT2AB acts as costimulator rather than as transcriptional modifier of terminal microglial phenotypes. We further found that, on average, 63.3% of transcriptional responses per trajectory were applicable to microglia carrying the *TREM2*^{R47H} variant, which binds endogenous ligands less effectively but can be activated by hT2AB; this points to an activation state–dependent effect of hT2AB on microglial fate. Interestingly, the highest number of hT2AB-induced gene expression changes was detected along the DAM trajectory (average number of genes/total analyzed: DAM = 552/1735, Cyc-M = 321/3353, IFN-R = 187/5005, and MHC-II = 148/4508), indicating that this trajectory was stimulated, but hT2AB treatment did not lead to full differentiation of the cells to a terminal phenotype in the time course of this experiment. Overall, transcriptional changes did not linearly translate into expansion of terminal cell types due to their dependency on the differentiation status prior to hT2AB-mediated stimulation.

Short-Term Treatment with mT2AB Impacts Microglial Proliferation and Activation Markers in *TREM2*^{R47H}-5XFAD. We next sought to determine the impact of anti-TREM2 treatment on brain biochemical and histological markers in 5XFAD animals. For this purpose, we utilized a murine IgG1 constant region chimeric variant of hT2AB (mT2AB). The 5-mo-old *TREM2*^{CV}-5XFAD and *TREM2*^{R47H}-5XFAD mice of both sexes were injected with a 30 mg/kg dose of mT2AB or control mIgG1 in the peritoneal cavity every 3 d for 10 d (Fig. 7*A*). At the end of the experiments, brains were divided into two halves: one half was lysed for biochemical measurement of soluble markers of microglial activation and proliferation including chemokines and cytokines, as well as Aβ peptides 1-40 and 1-42; the second half was sectioned to analyze Aβ coverage by confocal microscopy using anti-Aβ and Methoxy-04. Changes in chemokines and cytokines in hTREM2 transgenic mice on a 5XFAD background were consistent with those initially observed in hTREM2 transgenic mice on a wild-type background (Fig. 2), with induction of CCL4, CXCL10, and IL-1β observed in *TREM2*^{R47H}-5XFAD mice (Fig. 7*B*). Notably, mT2AB induced levels of CCL4, CXCL10, and IL-1β in *TREM2*^{R47H}-5XFAD mice comparable to the levels observed in *TREM2*^{CV}-5XFAD mice (Fig. 7*B*). Given that CCL4, CXCL10, and IL-1β are produced by microglia, these observations are consistent with scRNA-seq observations of increased proliferation and activation particularly of microglia expressing the *TREM2*^{R47H} variant. Aβ quantitation identified increased levels of amyloid deposition in females relative to males in both *TREM2*^{CV} and *TREM2*^{R47H} mice (*SI Appendix*, Fig. S5*A*). This result corroborated prior observations (25, 26) and extended them to mice carrying human TREM2, providing a potential explanation for the greater relative increases of microglial activation response genes in males observed after hT2AB treatment. Short-term treatment with mT2AB had no detectable impact on the total amount of plaque or soluble Aβ in either male or female mice, as measured by biochemical assessment of soluble or insoluble Aβ load (*SI Appendix*, Fig. S5*A*) and staining with anti-Aβ and Methoxy-04 (*SI Appendix*, Fig. S5 *B* and *C*). This is consistent with recent studies in which longer term treatment with TREM2 agonist antibodies resulted in robust induction of microglial barrier function and prevention of downstream neurotoxicity, without altering total

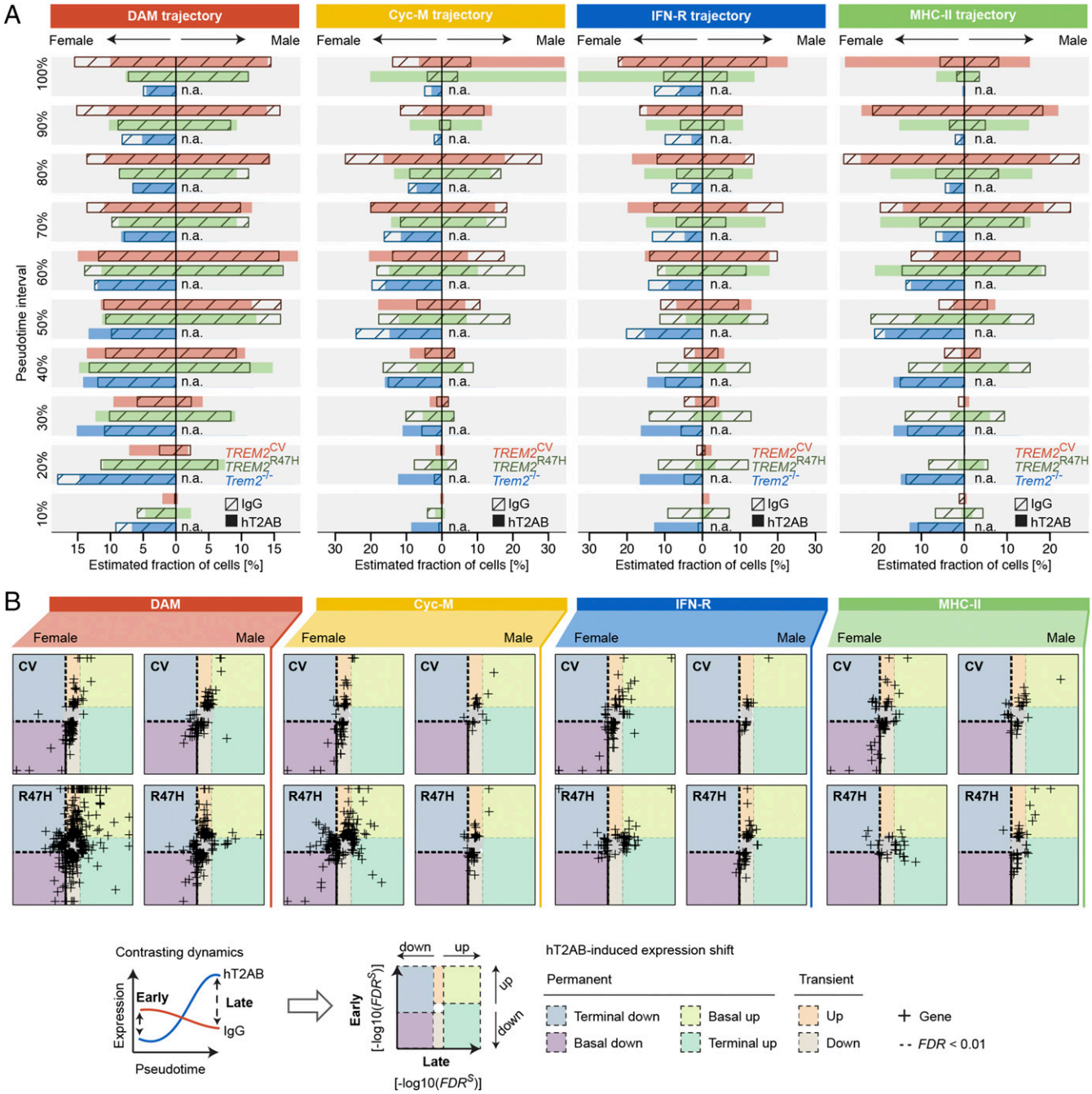

Fig. 6. hT2AB treatment effects on the microglia trajectory. (*A*) Estimated relative population sizes per time interval along each trajectory starting from the branching point toward the terminal end type. (*B*) Trajectory-based differential expression analysis of the early and late microglial differentiation stages. *P* values were calculated using Wald statistics and corrected for multiple testing via FDR. The FDR was weighted by the sign of the log fold-change *S* by FDR^S and -log10 transformed. Negative values denote hT2AB-induced down-regulation; positive values indicate up-regulation. Using an FDR cutoff of 0.01, transcriptional changes were classified into six categories: two transient with an early up-/down-regulation converging to baseline level and four permanent with either early and late up-/down-regulation or only late up-/down-regulation, respectively.

amyloid quantitation (25). It is possible that differences in the microglial response to amyloid or other AD pathologies can shed light on historical observations that total amyloid burden correlates poorly with cognition and that high levels of amyloid deposition can be observed in cognitively normal older adults (41, 42).

Discussion

In this study, we investigated the impact of amyloid deposition and an antihuman TREM2 agonist antibody on microglia activation, proliferation, and gene expression in $TREM2^{CV}$-5XFAD and $TREM2^{R47H}$-5XFAD mice. We first established a high-resolution single-cell profile of microglia in control hIgG1-treated $TREM2^{CV}$-5XFAD mice, demonstrating that microglia progressively differentiate from a homeostatic state into four distinct types in response to Aβ accumulation. These types include the previously reported DAM (9), IFN-R, and MHC-II (35), as well as Cyc-M. We showed that the relative distribution of microglial types depends on TREM2 genotype and mouse sex. In mice not

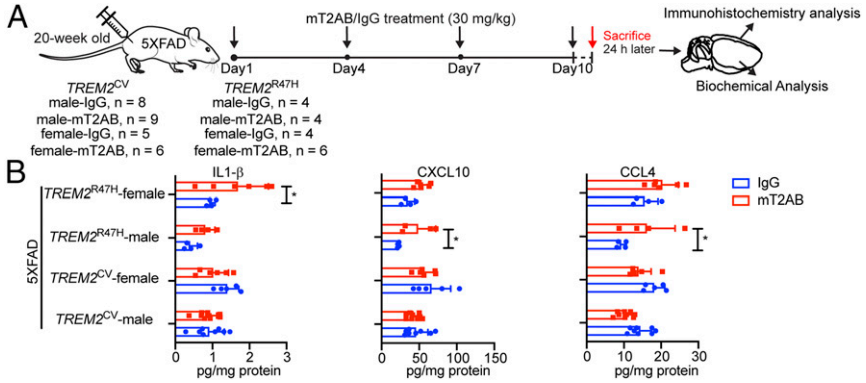

Fig. 7. Sustained acute treatment with mT2AB affects microglial responses to pathology differently. (*A*) Schematic diagram of mT2AB treatment in *TREM2*^{CV}-5XFAD or *TREM2*^{R47H}-5XFAD mice. The 20-wk-old mice were injected intraperitoneally with murine mT2AB at 30 mg/kg every 3 d for 10 d. Littermates were administered the same concentration of control mIgG1 antibody. Mice were killed 24 h after the last antibody injection and brains were harvested for immunohistochemistry and biochemical analysis. (*B*) Quantification of cytokines and chemokines, such as IL-1β, CXCL10, and CCL4 in the cortex lysates among different treatment groups. *$P < 0.05$; ***$P < 0.001$; ****$P < 0.0001$ by two-way ANOVA with Sidak's multiple comparisons test. Data are shown as mean ± SD. *TREM2*^{CV}-5XFAD, male, mIgG1, $n = 8$; *TREM2*^{CV}-5XFAD, male, mT2AB, $n = 9$; *TREM2*^{CV}-5XFAD, female, mIgG1, $n = 5$; *TREM2*^{CV}-5XFAD, female, mT2AB, $n = 6$; *TREM2*^{R47H}-5XFAD, male, mIgG1, $n = 4$; *TREM2*^{R47H}-5XFAD, male, mT2AB, $n = 4$; *TREM2*^{R47H}-5XFAD, female, mIgG1, $n = 4$; *TREM2*^{R47H}-5XFAD, female, mT2AB, $n = 6$.

treated with hT2AB, *TREM2*^{CV} was required for optimal differentiation of all types, which were conversely underrepresented in mice carrying the *TREM2*^{R47H} variant. Furthermore, IFN-R and Cyc-M were more abundant in female than male *TREM2*^{CV}-5XFAD mice, most likely reflecting the exacerbated Aβ accumulation in females. We next established the impact of hT2AB on microglial fates, demonstrating two major effects: hT2AB promoted the expansion of Cyc-M in mice with lower basal proliferation, including *TREM2*^{R47H}-5XFAD mice of both sexes and *TREM2*^{CV}-5XFAD male mice; moreover, hT2AB replenished the IFN-R and MHC-II cell pools in *TREM2*^{R47H}-5XFAD mice. Finally, in a short-term multidose scheme, mT2AB led to elevated brain content of chemokines in *TREM2*^{R47H}-5XFAD mice, which paralleled hT2AB-induced expansion of microglia.

One important conclusion of our study is that the activity of TREM2 seems saturable. Mice expressing *TREM2*^{R47H}, which is unable to effectively bind physiological ligands, had a clear defect in microglia cycling. However, engagement of *TREM2*^{R47H} with a surrogate ligand, such as hT2AB, markedly increased microglia proliferation. A similar result was recently corroborated with a different antihuman TREM2 mAb (25). In contrast, in mice expressing *TREM2*^{CV}, which binds endogenous ligands and promotes normal basal proliferation, hT2AB promoted only a modest increase of cycling of male microglia, which tend to proliferate less than female microglia because of less exposure to Aβ accumulation. This observation is important for future therapeutic applications of anti-TREM2 antibodies, as it suggests that these antibodies may be able to restore the impaired activation state observed in patients with hypofunctional mutations in TREM2 or that otherwise fail to mount a robust DAM response, as has been observed in some human AD postmortem brains. It also suggests that activation of microglia by TREM2 agonists is less likely to occur in the absence of injurious stimuli such as Aβ or alternate physiological TREM2 ligands.

It was previously shown that TREM2 is essential to induce full differentiation of DAM (9). Consistent with this, *TREM2*^{R47H}-5XFAD and *Trem2*$^{-/-}$-5XFAD mice had fewer DAM. Our data extend this concept to IFN-R and MHC-II microglia, which were also less abundant in *TREM2*^{R47H}-5XFAD and *Trem2*$^{-/-}$-5XFAD mice than in *TREM2*^{CV}-5XFAD mice. Importantly, our study also demonstrates that TREM2 signaling, although necessary, is not sufficient to induce the various terminal microglial types, which is consistent with prior reports of two-step activation of the DAM phenotype (9). Microglia cell fate is first driven by shifting neuropathological conditions that trigger signaling pathways that furcate and coopt TREM2 to sustain expansion toward four terminal cell types. Accordingly, hT2AB induced transcriptional changes proximal to the branching point, as soon as cell fate decisions are made, suggesting that hT2AB may stimulate common pathways in each trajectory that facilitate progression toward terminal microglial types. Given our previous demonstration that TREM2 sustains the mTOR pathway, TREM2 signaling may costimulate preactivated pathways by providing building blocks and energy required for microglial responses to Aβ or other injuries (43).

In a short-term multidose scheme consisting of frequent administrations of high mAb doses within 10 d, mT2AB induced responses consistent with microglial proliferation and activation which differed by TREM2 genotype and sex, presumably in relation to the reduced levels of TREM2 engagement in *TREM2*^{R47H} and male mice. Our report is consistent with a recent study in which a long term treatment of *TREM2*^{CV}-5XFAD and *TREM2*^{R47H}-5XFAD mice with a different antihuman TREM2 mAb resulted in expansion of metabolically active and proliferating microglial populations to a greater extent in *TREM2*^{R47H}-5XFAD than *TREM2*^{CV}-5XFAD (25) and in a 12-wk experimental paradigm led to changes consistent with the induction of a more effective microglial barrier response including changes in plaque compaction, alterations of microglial-plaque association, and reductions in neurite dystrophy consistent with reduced neurotoxicity of Aβ.

In conclusion, our in vivo evaluation of the antihuman TREM2 mAb hT2AB shows that systemic administration of this antibody in *TREM2*^{CV}-5XFAD and *TREM2*^{R47H}-5XFAD in vivo 1) replenished the Cyc-M, IFN-R, and MHC-II pools in *TREM2*^{R47H}-5XFAD mice; 2) brought the representation of male Cyc-M and IFN-R microglia closer to that of females in *TREM2*^{CV}-5XFAD mice, in which microglia transitioning had already been robustly activated; and 3) costimulated common pathways in each trajectory that facilitate progression toward terminal microglial types.

Methods

Experimental details on animals, survival assay of BMMs, GFP reporter assay, pharmacodynamics and pharmacokinetics of hT2AB, immunostaining for Aβ and image analyses, and Aβ and chemokine/cytokines quantification are described in detail in *SI Appendix, SI Methods*.

Animals. All animal experiments were conducted in compliance with Institutional regulations, under authorized protocols #20160220 and 19-0981 approved by the Institutional Animal Care and Use Committee of Washington University and Amgen South San Francisco.

Generation of Fully Human Anti-hTREM2 Antibodies. hT2AB and mT2AB antibodies to hTREM2 were generated by gene-gun immunization of XMG2-K and XMG2-KL XenoMouse transgenic mice (29, 44) with a cDNA encoding human TREM2 and DAP12. Antibody selection and generation was performed as described in *SI Appendix, SI Methods*.

Syk Phosphorylation Assay to Assess TREM2 Activation. A HEK293-based stable cell line expressing hTREM2 and hDAP12 (clone G13) or hMacs were used for antibody activity assessment as described in *SI Appendix*, SI Methods. The antibody activity (stimulation) was reported as fold of control (S/B): S/B = Sample pSyk signal (counts)/Basal pSyk signal (isotype control pSyk signal counts). The EC_{50} of hT2AB was determined by a four-parameter logistic fit model of GraphPad Prism Version 6.07.

Measurement of sTREM2 and CCL4 Levels in hMacs by MSD. hMacs were used for measuring the CCL4 and sTREM2 in conditioned media after treatment with hT2AB or hIgG1 isotype control antibody, as described in *SI Appendix, SI Methods*. Acetylated LDL was used as a positive control for each group of CCL4 measurement.

Single-Cell RNA-Seq. Eight-mo-old mice were injected intraperitoneally with hT2AB or control hIgG1 at 30 mg/kg 48 h before being killed. After perfusion with cold PBS, cortices were dissociated, and CD45+ cells were sorted using FACS. All CD45+ cell libraries were prepared using the 10× Genomics Chromium Single Cell 3′ v2 Gene Expression Kit and sequenced on Illumina NovaSeq. 6000 flow cells to achieve a read depth of 50,000 reads per cell. Data were analyzed as described in *SI Appendix*, SI Methods. Samples that did not exhibit hT2AB exposure were excluded from downstream analyses. Sequencing data and sample quality reports can be obtained from Gene Expression Omnibus under series number GSE156183.

Statistical Analyses. All graphs represent the mean of all samples in each group ±SD or SEM as indicated in the figure legends. GraphPad Prism software (v8) was used to perform statistical analyses. $P < 0.05$ was considered significant difference between different treatment groups, determined by two-way ANOVA with Sidak's multiple comparisons test, unless otherwise indicated.

Data Availability. All study data are included in the article and supporting information.

ACKNOWLEDGMENTS. We thank Ramsay Macdonald and Ai Ching Lim for providing reagents for the studies, David Tran for culturing of human macrophages, Laura Sekirov for measuring antibody affinities, and Oliver Homann and Songli Wang for comments on the scRNA-seq data analysis.

1. J. M. Long, D. M. Holtzman, Alzheimer disease: An update on pathobiology and treatment strategies. *Cell* **179**, 312–339 (2019).
2. D. J. Selkoe, J. Hardy, The amyloid hypothesis of Alzheimer's disease at 25 years. *EMBO Mol. Med.* **8**, 595–608 (2016).
3. M. T. Heneka, Microglia take centre stage in neurodegenerative disease. *Nat. Rev. Immunol.* **19**, 79–80 (2019).
4. R. E. Tanzi, L. Bertram, Twenty years of the Alzheimer's disease amyloid hypothesis: A genetic perspective. *Cell* **120**, 545–555 (2005).
5. C. M. Karch, A. M. Goate, Alzheimer's disease risk genes and mechanisms of disease pathogenesis. *Biol. Psychiatry* **77**, 43–51 (2015).
6. S. Carmona, J. Hardy, R. Guerreiro, *The Genetic Landscape of Alzheimer Disease* (Elsevier B.V., ed. 1, 2018).
7. I. E. Jansen *et al.*, Genome-wide meta-analysis identifies new loci and functional pathways influencing Alzheimer's disease risk. *Nat. Genet.* **51**, 404–413 (2019).
8. P. Yuan *et al.*, TREM2 Haplodeficiency in mice and humans impairs the microglia barrier function leading to decreased amyloid compaction and severe axonal dystrophy. *Neuron* **90**, 724–739 (2016).
9. H. Keren-Shaul *et al.*, A unique microglia type Associated with restricting development of alzheimer's disease. *Cell* **169**, 1276–1290.e17 (2017).
10. S. Krasemann *et al.*, The TREM2-APOE pathway drives the transcriptional phenotype of dysfunctional microglia in neurodegenerative diseases. *Immunity* **47**, 566–581.e9 (2017).
11. Y. Zhou *et al.*, Human and mouse single-nucleus transcriptomics reveal TREM2-dependent and TREM2-independent cellular responses in Alzheimer's disease. *Nat. Med.* **26**, 131–142 (2020).
12. K. Srinivasan *et al.*, Alzheimer's patient microglia exhibit enhanced aging and unique transcriptional activation. *Cell Rep.* **31**, 107843 (2020).
13. T. K. Ulland, M. Colonna, TREM2–A key player in microglial biology and Alzheimer disease. *Nat. Rev. Neurol.* **14**, 667–675 (2018).
14. P. Wunderlich *et al.*, Sequential proteolytic processing of the triggering receptor expressed on myeloid cells-2 (TREM2) protein by ectodomain shedding and γ-secretase-dependent intramembranous cleavage. *J. Biol. Chem.* **288**, 33027–33036 (2013).
15. P. Thornton *et al.*, TREM2 shedding by cleavage at the H157-S158 bond is accelerated for the Alzheimer's disease-associated H157Y variant. *EMBO Mol. Med.* **9**, 1366–1378 (2017).
16. R. Guerreiro *et al.*; Alzheimer Genetic Analysis Group, TREM2 variants in Alzheimer's disease. *N. Engl. J. Med.* **368**, 117–127 (2013).
17. T. Jonsson *et al.*, Variant of TREM2 associated with the risk of Alzheimer's disease. *N. Engl. J. Med.* **368**, 107–116 (2013).
18. Y. Wang *et al.*, TREM2 lipid sensing sustains the microglial response in an Alzheimer's disease model. *Cell* **160**, 1061–1071 (2015).
19. W. M. Song *et al.*, Humanized TREM2 mice reveal microglia-intrinsic and -extrinsic effects of R47H polymorphism. *J. Exp. Med.* **215**, 745–760 (2018).
20. Y. Wang *et al.*, TREM2-mediated early microglial response limits diffusion and toxicity of amyloid plaques. *J. Exp. Med.* **213**, 667–675 (2016).
21. T. R. Jay *et al.*, Disease progression-dependent effects of TREM2 deficiency in a mouse model of Alzheimer's disease. *J. Neurosci.* **37**, 637–647 (2017).
22. C. Y. D. Lee *et al.*, Elevated TREM2 gene dosage reprograms microglia responsivity and ameliorates pathological phenotypes in alzheimer's disease models. *Neuron* **97**, 1032–1048.e5 (2018).
23. Q. Cheng *et al.*, TREM2-activating antibodies abrogate the negative pleiotropic effects of the Alzheimer's disease variant *Trem2*^{R47H} on murine myeloid cell function. *J. Biol. Chem.* **293**, 12620–12633 (2018).
24. K. Schlepckow *et al.*, Enhancing protective microglial activities with a dual function TREM2 antibody to the stalk region. *EMBO Mol. Med.* **12**, e11227 (2020).
25. S. Wang *et al.*, Anti-human TREM2 induces microglia proliferation and reduces pathology in an Alzheimer's disease model. *J. Exp. Med.* **217**, e20200785 (2020).
26. H. Oakley *et al.*, Intraneuronal β-amyloid aggregates, neurodegeneration, and neuron loss in transgenic mice with five familial alzheimer's disease mutations: Potential factors in amyloid plaque formation. *J. Neurosci.* **26**, 10129–10140 (2006).
27. K. R. Sadleir, W. A. Eimer, S. L. Cole, R. Vassar, Aβ reduction in BACE1 heterozygous null 5XFAD mice is associated with transgenic APP level. *Mol. Neurodegener.* **10**, 1–16 (2015).
28. S. Bhattacharya, C. Haertel, A. Maelicke, D. Montag, Galantamine slows down plaque formation and behavioral decline in the 5XFAD mouse model of Alzheimer's disease. *PLoS One* **9**, e89454 (2014).
29. M. J. Mendez *et al.*, Functional transplant of megabase human immunoglobulin loci recapitulates human antibody response in mice. *Nat. Genet.* **15**, 146–156 (1997).
30. K. Otero *et al.*, Macrophage colony-stimulating factor induces the proliferation and survival of macrophages via a pathway involving DAP12 and β-catenin. *Nat. Immunol.* **10**, 734–743 (2009).
31. T. S. P. Heng, M. W. Painter; Immunological Genome Project Consortium, The immunological genome project: Networks of gene expression in immune cells. *Nat. Immunol.* **9**, 1091–1094 (2008).
32. D. Gate *et al.*, Clonally expanded CD8 T cells patrol the cerebrospinal fluid in Alzheimer's disease. *Nature* **577**, 399–404 (2020).
33. A. Scialdone *et al.*, Computational assignment of cell-cycle stage from single-cell transcriptome data. *Methods* **85**, 54–61 (2015).
34. X. Xu *et al.*, IFN-stimulated gene LY6E in monocytes regulates the CD14/TLR4 pathway but inadequately restrains the hyperactivation of monocytes during chronic HIV-1 infection. *J. Immunol.* **193**, 4125–4136 (2014).
35. H. Mathys *et al.*, Temporal tracking of microglia activation in neurodegeneration at single-cell resolution. *Cell Rep.* **21**, 366–380 (2017).
36. K. Van den Berge *et al.*, Trajectory-based differential expression analysis for single-cell sequencing data. *Nat. Commun.* **11**, 1201 (2020).
37. K. Kurakula, D. S. Koenis, C. M. van Tiel, C. J. M. de Vries, NR4A nuclear receptors are orphans but not lonesome. *Biochim. Biophys. Acta* **1843**, 2543–2555 (2014).
38. R. N. Hanna *et al.*, The transcription factor NR4A1 (Nur77) controls bone marrow differentiation and the survival of Ly6C- monocytes. *Nat. Immunol.* **12**, 778–785 (2011).
39. N. Ipseiz *et al.*, The nuclear receptor Nr4a1 mediates anti-inflammatory effects of apoptotic cells. *J. Immunol.* **192**, 4852–4858 (2014).
40. C. K. Glass, K. Saijo, Nuclear receptor transrepression pathways that regulate inflammation in macrophages and T cells. *Nat. Rev. Immunol.* **10**, 365–376 (2010).
41. R. D. Terry *et al.*, Physical basis of cognitive alterations in alzheimer's disease: Synapse loss is the major correlate of cognitive impairment. *Ann. Neurol.* **30**, 572–580 (1991).
42. K. M. Rodrigue, K. M. Kennedy, D. C. Park, Beta-amyloid deposition and the aging brain. *Neuropsychol. Rev.* **19**, 436–450 (2009).
43. T. K. Ulland *et al.*, TREM2 maintains microglial metabolic fitness in alzheimer's disease. *Cell* **170**, 649–663.e13 (2017).
44. L. L. Green *et al.*, Antigen-specific human monoclonal antibodies from mice engineered with human Ig heavy and light chain YACs. *Nat. Genet.* **7**, 13–21 (1994).